

The Effect of Solute Nb on the Austenite-to-Ferrite Transformation

TAO JIA and MATTHIAS MILITZER

Niobium is a widely used micro-alloying element in steels that can retard the austenite-to-ferrite transformation primarily by solute drag when Nb remains in solution. It is critical to develop quantitative models to predict the effect of Nb on the transformation kinetics. In the present work, dedicated continuous cooling transformation (CCT) studies were performed for a low-carbon steel microalloyed with 0.047 wt pct Nb starting from fully recrystallized austenite states with the same grain size but different amounts of Nb in solution. The austenite-to-ferrite transformation kinetics is described from a fundamental perspective by assuming a mixed-mode reaction including solute drag of Nb. Using the solute drag model of Fazeli and Militzer, the intrinsic interface mobility, trans-interface diffusivity of Nb, and its binding energy to the interface have been determined from the CCT data. The interfacial parameters are critically analyzed and compared with independent measurements of diffusion and grain boundary segregation.

DOI: 10.1007/s11661-014-2659-5

© The Minerals, Metals & Materials Society and ASM International 2014

I. INTRODUCTION

SINCE the 1960's microalloying with Nb has been widely used to enable thermo-mechanical controlled processing of steels. The beneficial effects of Nb are related to the fact that it forms carbides due to its strong interaction with carbon thereby producing Zener pinning on boundary motion and precipitation strengthening, while solute Nb has a strong tendency to segregate to grain or interphase boundaries because of the large lattice misfit of Nb atoms in Fe which leads to a solute drag effect on boundary motion. Regardless of Nb state in austenite, it is generally accepted that Nb delays austenite recrystallization thereby enabling controlled rolling below the recrystallization stop temperature.^[1] As a result, pancaked austenite is present at the exit of finish rolling and leads upon cooling to the refinement of the final microstructure. In detail, the Nb state prior to phase transformation, however, may have for a given austenite structure two opposite effects on the austenite decomposition kinetics and resulting microstructure. When Nb forms precipitates, it can promote the ferrite or bainite transformation by removal of solute Nb thereby decreasing the solute drag effect, and possibly by providing potential nucleation sites.^[2-4] On the other hand, solute Nb delays the phase transformation as has been extensively investigated.^[3-8] The mechanisms of these delays have been

discussed in terms of the potential effects of Nb on both nucleation and growth of ferrite. The segregation of Nb to austenite grain boundaries reduces their energy and, thus, decreases their potency as heterogeneous nucleation sites for ferrite. Further, the strong interaction of Nb with carbon decreases the diffusivity of carbon as it is partitioned from ferrite nuclei to austenite. Alternatively, the retarding effect of Nb on the ferrite transformation is primarily attributed to the solute drag mechanism.^[3-5] Even though the role of Nb on phase transformation is of significant practical relevance, modeling the effect of solute Nb on the austenite decomposition kinetics has drawn comparatively little attention so far. There have been dedicated research efforts over the past decade to better understand the interaction of alloying element with migrating interfaces (Alemi).^[9] For Fe-based alloys, these research efforts have primarily emphasized elements like Ni,^[10-13] Cr,^[14] Mo,^[12,13] Si^[15] and Mn.^[13,16-21]

Gómez *et al.*^[22] and Majta *et al.*^[23] used the Johnson–Mehl–Avrami–Kolmogorov (JMAK) approach to model the phase transformation in Nb-containing steels due to its simplicity and numerical convenience. But the effect of Nb on the underlying nucleation and growth is not explicitly accounted for, and the model is only valid for the investigated steel compositions and experimental conditions. Alternatively, attempts have been made to incorporate the Nb effect from a fundamental perspective. Lee *et al.*^[7] used the classical nucleation and carbon-diffusion controlled growth theories to describe the austenite-to-ferrite transformation kinetics in Nb-containing steels. The solute drag effect of Nb is implicitly considered by assuming that the activation energy of carbon diffusivity is a function of solute Nb content such that carbon diffusion is reduced with increasing the Nb solute level. A more rigorous mixed-mode model was developed and has been widely applied to Fe-C-X alloys (X being a substitutional element like Mn, Cr and Nb).

TAO JIA, formerly Postdoctoral Fellow with the Centre for Metallurgical Process Engineering, The University of British Columbia, 309-6350 Stores Rd., Vancouver, BC V6T1Z4, Canada, is now Associate Professor with the State Key Laboratory of Rolling and Automation, Northeastern University, P.O. Box No. 105, Shenyang, 110004 Liaoning, P.R. China. Contact e-mail: tao.jia.81@gmail.com
MATTHIAS MILITZER, Professor, is with the Centre for Metallurgical Process Engineering, The University of British Columbia.

Manuscript submitted March 27, 2014.

Article published online November 19, 2014

Here, both long-range carbon diffusion and interface reaction are assumed to control the transformation rate. In this modeling framework, the interface velocity is expressed as the product of the local chemical driving pressure and an effective interface mobility. This effective term can be used to account for the role of alloying element X on the interface migration rate.^[24,25] Mecozzi *et al.*^[26] and Takahama *et al.*^[27] have used phase field modeling (PFM) to simulate the austenite-to-ferrite transformation in a Nb-containing steel. In these PFM simulations, it is assumed that the interface mobility has an Arrhenius relationship with an activation energy of 140 kJ/mol^[28] and the pre-exponential mobility term is employed as an adjustable parameter to replicate continuous cooling transformation (CCT) data. Takahama *et al.*^[27] expressed the obtained effective interface mobility with solute drag and pinning pressure terms that are consistent with the dissolution of NbC as a function of the austenitization temperature. In particular, they found that the solute drag strength is large at intermediate interface velocities for the investigated cooling rate of 0.3 K/s. In a number of PFM simulations, the fitted effective interface mobility exhibits a cooling rate dependence.^[16,17] This non-physical behavior can be mitigated by incorporating solute drag in a more rigorous way whereby the interface mobility becomes a function of both temperature and interface velocity.^[29] Here, solute drag may be accounted by describing the interface velocity in terms of an intrinsic temperature-dependent interface mobility in combination with a solute drag pressure that effectively reduces the chemical driving pressure as a function of both temperature and interface velocity. For example, Fazeli and Militzer^[18] and Jia and Militzer^[19] had used this approach to describe the austenite-to-ferrite transformation in low-carbon steels and Fe-Mn alloys. This analysis has yet to be applied to Nb microalloyed steels despite their technological importance.

The present work describes a dedicated CCT study for a low-carbon steel microalloyed with 0.047 wt pct Nb starting from fully recrystallized austenite states with the same grain size but different levels of Nb in solution. Based on these studies, the effect of Nb on the phase transformation kinetics is quantified to extract the solute drag parameters for Nb, *i.e.*, the binding energy and the diffusivity across the interface, that are used in a mixed-mode model to describe the observed austenite-to-ferrite transformation kinetics. The paper concludes with a critical analysis of the proposed modeling approach.

II. MATERIAL AND EXPERIMENTAL PROCEDURES

An X65 commercial linepipe steel microalloyed with Nb was employed in the present study. Table I shows the chemistry of the investigated steel. Using Thermo-

Calc with the Fe2000 database, the A_{e3} temperature was determined to be 1112 K (839 °C). Tensile samples with a cylindrical working zone of 10 mm length and 6 mm diameter were machined along the rolling direction from the as-received hot-rolled material.

The CCT tests were conducted on a GLEEBLE 3500 thermo-mechanical simulator. The thermo-mechanical processing path employed in these tests is schematically shown in Figure 1. Based on a previous study,^[30] the samples were first austenitized at 1473 K (1200 °C) for 2 minutes to dissolve all NbC precipitates. Then a grain refinement step was executed at 1323 K (1050 °C) by deforming the sample in axisymmetric compression at a rate of 1 s^{-1} to a true strain of 0.3 followed by holding of 20 seconds to produce a fully recrystallized austenite microstructure with a grain size of 40 μm . Subsequently, the samples were rapidly cooled to 1173 K (900 °C) at a rate of 100 K/s and then held for either 0, 2, or 20 minutes to achieve different levels of Nb in solution by partial re-precipitation of NbC. Finally, the samples were cooled from 1173 K (900 °C) at constant rates of 1, 2 and 5 K/s, respectively. During cooling, the austenite decomposition was monitored with a dilatometer at the center of the sample, where also a K-type thermocouple was spot welded to measure the temperature. The austenite decomposition kinetics was determined from the dilation data (*i.e.*, the radial expansion of the sample) using the lever rule as well as the method proposed by Bhadeshia *et al.*^[31] Both analysis techniques provide fractions transformed that are within the experimental errors of the dilation measurements (± 0.05) and the results presented here are based on the lever rule method. Further, the final microstructure of all CCT samples was analyzed using conventional metallographic techniques including grinding, polishing, and etching with 2 pct Nital. Optical micrographs of the etched surfaces were used to measure the ferrite fraction

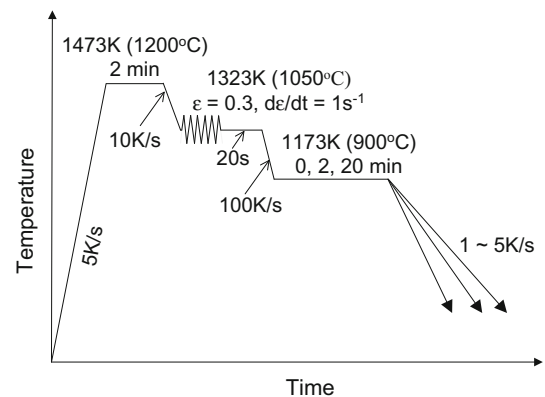


Fig. 1—Experimental procedure for Gleeble tests.

Table I. Chemistry of the Investigated Steel (in Weight Percent)

C	Mn	Si	P	S	Al	Nb	N
0.06	1.49	0.2	0.009	0.002	0.038	0.047	0.0094

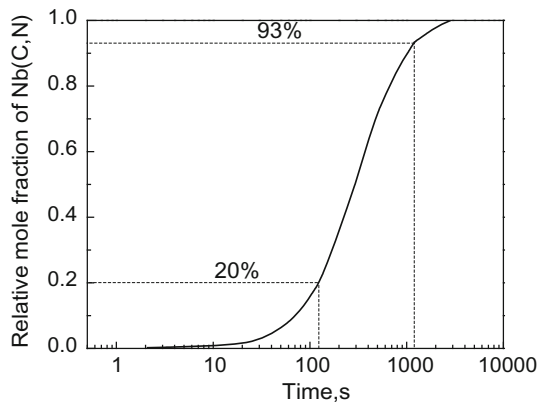


Fig. 2—Estimation of NbC re-precipitation at 1173 K (900 °C) based on the precipitation kinetics data of Park *et al.*^[32]

in each sample, using the point count method outlined in the ASTM standard E 562.

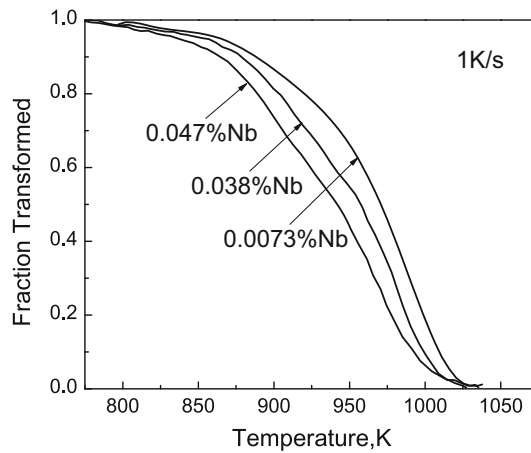
The amount of Nb in solution was estimated from the precipitation kinetics study by Park *et al.*^[32] who investigated a Nb microalloyed steel with a comparable chemistry, *i.e.*, Fe-0.08C-1.21Mn-0.2Si-0.038Nb-0.0017N (see Figure 2). For the present steel, the amount of Nb in solution was concluded to be 0.047, 0.038 and 0.0073 wt pct after 0, 2 and 20 minutes holding at 1173 K (900 °C), respectively.

III. RESULTS AND DISCUSSION

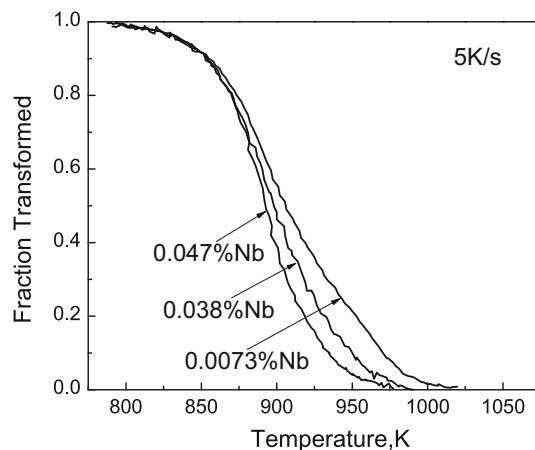
A. Experimental Observations

Figure 3 shows the overall austenite decomposition kinetics for a given cooling rate (*i.e.*, 1 and 5 K/s, respectively) and different levels of Nb in solution. The retarding effect of Nb in solution on the transformation is obvious. For example, at a cooling rate of 1 K/s, the entire transformation is consistently shifted to lower temperature by about 15 K when the solute Nb content is increased from 0.0073 to 0.038 wt pct and by about another 15 K when the solute Nb content is further increased to 0.047 wt pct. The temperatures for 50 pct transformed decreases from 973 K to 943 K (700 °C to 670 °C). At the higher cooling rate of 5 K/s, the overall transformation temperatures are lower with 50 pct transformation observed at around 898 K (625 °C). Here, the delay of the transformation due to Nb in solution is only evident in the initial portion of transformation (below 50 pct transformed), *e.g.*, the transformation start temperatures (quantified as 5 pct transformed) decrease from 982 K to 947 K (709 °C to 674 °C) when the Nb content in solution is increased from 0.0073 to 0.047 wt pct. For later stages, however, the transformation temperatures become independent of the Nb content in solution and the austenite decomposition is completed in all three cases at 793 K (520 °C) (see Figure 3(b)).

Figure 4 shows the optical micrographs for both cooling rates and the cases with the minimum and maximum levels of Nb in solution (0.0073 and 0.047 wt pct). As expected, the lowering of the transformation temperature due to either increasing the



(a)



(b)

Fig. 3—Austenite decomposition kinetics for different levels of Nb in solution (in weight percent) at cooling rates of (a) 1 K/s and (b) 5 K/s, respectively.

cooling rate or the amount of Nb in solution is evident in the resulting microstructures. In case of the highest transformation temperature (1 K/s, 0.0073 wt pct Nb), the microstructure is primarily ferrite with some pearlite and bainite (Figure 4(a)). Increasing the Nb content in solution for cooling at 1 K/s decreases the ferrite fraction and increases the bainitic portion (Figure 4(b)). For the higher cooling rate (5 K/s), the microstructures become dominantly bainitic consistent with the overall lower transformation temperatures. For the case with the lower content of Nb in solution, a ferrite rim outlining the prior austenite grain boundaries are clearly visible (Figure 4(c)), whereas the fraction of allotriomorphic ferrite is greatly reduced when the amount of Nb in solution is maximized (Figure 4(d)).

B. Model for Austenite-to-Ferrite Transformation

Here, a model is proposed to account for the effect of Nb in solution on the austenite-to-ferrite transformation, *i.e.*, the initial portion of the transformation until the metallographically measured ferrite fraction is reached. It is assumed that pearlite and/or bainite form in the later transformation stages, which is consistent with a

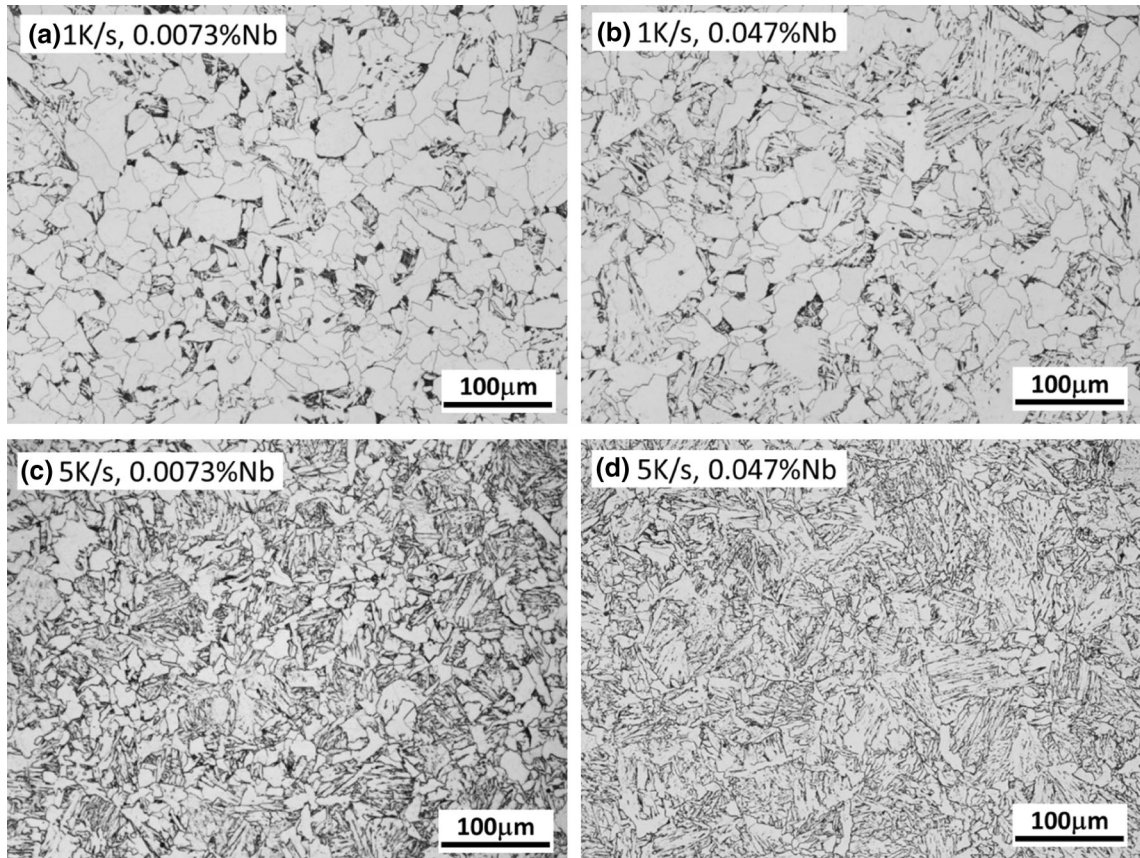


Fig. 4—Optical micrographs of CCT samples for the indicated experimental conditions.

sequential formation of different transformation products. The observed effect of Nb in solution is of kinetic nature as Nb is a ferrite stabilizer and bringing more Nb in solution should from a thermodynamic aspect promote ferrite formation. The amount of Nb in solution is, however, sufficiently small for all three cases that its effect on equilibrium transformation temperatures is negligible.

A model for ferrite transformation start (5 pct transformed) has previously been proposed^[33,34] and applied to the present steel.^[35] Thus, the present analysis emphasizes the ferrite growth stage above a ferrite fraction of 0.05.

The effect of Nb on ferrite growth can be described with a mixed-mode model that combines long-range carbon diffusion in austenite with the interface reaction incorporating solute drag. The interface velocity is calculated by

$$v = M(\Delta G_{\text{chem}} - \Delta G_{\text{SD}}), \quad [1]$$

where M is the intrinsic interface mobility, ΔG_{chem} is the chemical driving pressure, and ΔG_{SD} is the solute drag pressure. Using ThermoCalc with the Fe2000 database, ΔG_{chem} is calculated by assuming a constrained equilibrium condition as reference ($\Delta G_{\text{chem}} = 0$) where substitutional elements remain configurationally frozen while the equality of the chemical potential of carbon across the interface is maintained.^[18]

The solute drag pressure, due to the asymmetrical distribution of solutes with a concentration C_S in the interface, is calculated according to the model proposed

by Fazeli and Miltzer.^[18] In this solute drag model, dimensionless variables for concentration, distance and velocity are defined, *i.e.*, $C = C_S/C_{S,0}$, $X = x/\delta$ and $V = v\delta/D_b$. Here, $C_{S,0}$ is the bulk solute content, x is the position in the interface, δ is half of the interface thickness, and D_b is the trans-interface diffusivity of the solute. An asymmetrical wedge-shaped well is used for the interaction potential, E , of solutes with the interface such that the potential gradient within the interface is given by

$$\begin{cases} \partial E/\partial X = \Delta E - E_0 & -1 < X < 0 \\ \partial E/\partial X = \Delta E + E_0 & 0 < X < 1 \end{cases} \quad [2]$$

where E_0 is the solute-interface binding energy and ΔE is half of the chemical potential difference for the solute in austenite and ferrite. Here, the binding energy is given in positive numbers as in previous work^[19] to characterize the strength of the attractive solute-interface interaction. Then, the segregation profile of Nb can be determined by solving the following differential equation

$$\frac{\partial C_{\text{new}}}{\partial X} + \frac{C_{\text{new}}}{RT} \frac{\partial E}{\partial X} \Big|_{\text{new}} + V \left(C_{\text{new}} - \exp\left(\frac{\Delta E}{RT} X\right) \right) = 0, \quad [3]$$

where effective concentration and potential gradient terms, *i.e.*, C_{new} and $\partial E/\partial X|_{\text{new}}$ are introduced such that^[18]

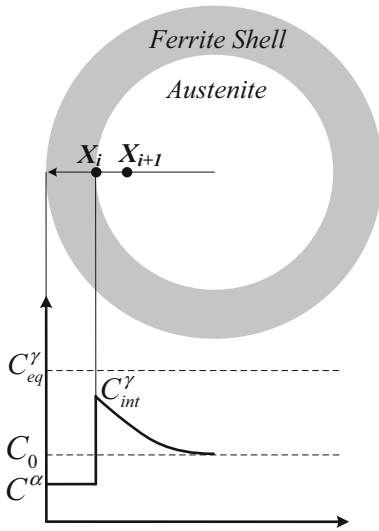


Fig. 5—Schematic illustration of the spherical geometry used in the kinetic model.

$$C_{\text{new}} = C \exp\left(\frac{\Delta E}{RT} X\right) \quad [4]$$

$$\left.\frac{\partial E}{\partial X}\right|_{\text{new}} = \frac{\partial E}{\partial X} - \Delta E \quad [5]$$

to avoid the artifact of residual solute drag at zero interface velocity. By integrating the contribution from all solute atoms segregated at the moving interface, the solute drag pressure is calculated as^[18]

$$\Delta G_{\text{SD}} = -C_{\text{S},0} \int_{-1}^1 (C_{\text{new}} - 1) \left.\frac{\partial E}{\partial X}\right|_{\text{new}} dX \quad [6]$$

Secondly, in order to link the interface motion with the transformed ferrite fraction, a suitable assumption for the growth geometry is required. As clearly seen in the micrograph shown in Figure 4(c), ferrite forms in early transformation stages films along prior austenite grain boundaries and grows inwards to consume the parent austenite grain. A suitable geometry to describe this situation is a spherical austenite grain with an outer ferrite shell growing toward the grain interior as schematically illustrated in Figure 5. This is relevant for cooling scenarios where nucleation site saturation occurs at austenite grain boundaries and the overall kinetics is mainly controlled by subsequent thickening of the ferrite shell.

The flowchart of the overall calculation process is shown in Figure 6. In the program, the spherical austenite grain is equally divided into 500 segments in radial direction to solve the diffusion equation for carbon in austenite. The initial condition is to have 100 pct austenite with a flat carbon profile replicating the nominal carbon content. The calculation is initiated such that the experimental transformation start temperature for 5 pct transformed is matched with the simulation. In the first time step, it is assumed that the outer

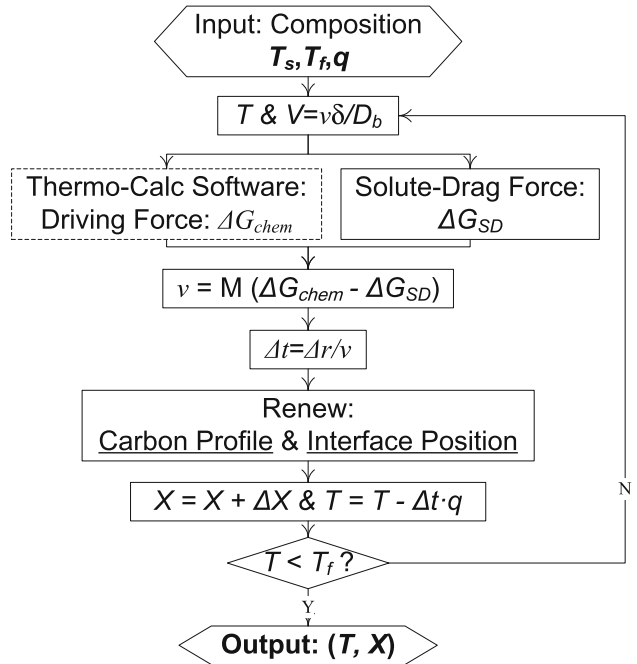


Fig. 6—Flowchart of the calculation program for phase transformation.

shell node is exposed to the chemical driving pressure, ΔG_{chem} , of the austenite-ferrite transformation for the nominal carbon content and initial temperature that is approximately 10 K above the experimental transformation start temperature (5 pct transformed). The subsequent simulation procedures are the same for all time steps, *i.e.*, ΔG_{chem} and ΔG_{SD} are first calculated based on the carbon diffusion profile and interface velocity from the previous time step. Then, the interface velocity is determined by Eq. [1] to obtain the time step length required for the interface moving forward one segment, Δr , at the given temperature. Next, the associated change of the carbon diffusion profile in austenite is calculated by using an implicit finite difference method. The program then enters into the next calculation cycle until the ferrite transformation stop temperature T_f is reached where ferrite formation ceases as concluded from the experimental CCT data.

In addition to the binding energy, the main parameters employed in the kinetic model include the intrinsic interface mobility and the trans-interface diffusivity, D_b , of Nb, normalized by the interface thickness, *i.e.*

$$M = M_0 \exp\left(-\frac{Q}{RT}\right) \quad [7]$$

$$\frac{D_b}{\delta} = \frac{D_0}{\delta} \exp\left(-\frac{Q_b}{RT}\right), \quad [8]$$

where M_0 and D_0 are the pre-exponential factors and Q and Q_b are the activation energies, respectively. As proposed when analyzing the austenite-to-ferrite transformation in the Fe-Mn system,^[19] D_0 and Q are taken from the literature, whereas M_0 and Q_b are employed as adjustable parameters. The pre-exponential factor D_0

Table II. Adjustable Ferrite Growth Parameters

M_0 (cm mol/J s)	Q_b (kJ/mol)	E_0 (kJ/mol)
2.5	263	48

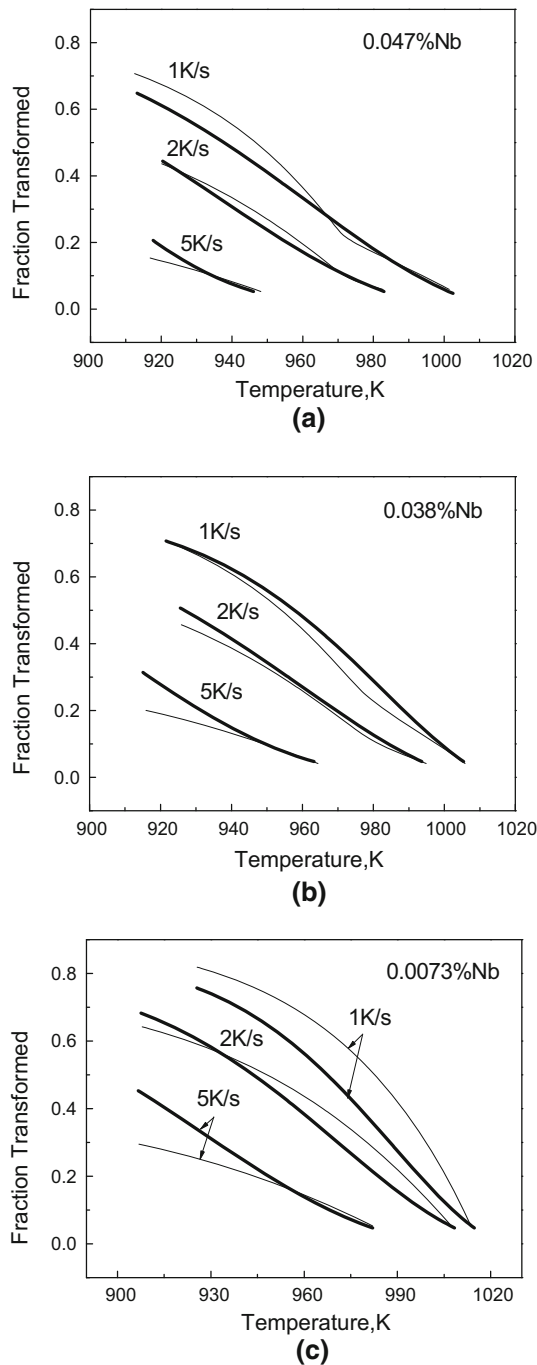


Fig. 7—Comparison between simulated (thin lines) and measured (thick lines) phase transformation kinetics.

has been chosen as the geometric mean of the values for Nb bulk diffusion in ferrite^[36,37] and austenite.^[38] By taking an interface width of 1 nm, the D_0/δ is calculated to be 33.5×10^7 cm/s. For the activation energy Q of

the intrinsic mobility 140 kJ/mol^[28] is adopted as in previous studies.^[18,19]

In summary, there are three adjustable parameters in the currently used model, *i.e.*, M_0 , Q_b , and E_0 that are determined to provide the best fit of the austenite-to-ferrite transformation kinetics. The present ferrite growth simulations start with an initial ferrite fraction of 0.05 at the measured transformation start temperature, *i.e.*, they agree per definition with the experimental data at the selected start condition. The simulations conclude at the experimental ferrite stop temperature and then the primary fit criterion is to minimize the overall difference of ferrite fraction between the simulations and the experimental data for the nine CCT cases. Following the steps described above, the parameter set is obtained as shown in Table II which gives the best agreement between experimentally measured kinetics and model calculations. As illustrated in Figure 7, the agreement that is obtained in this way between simulation and experimental results is, in general, good, in particular when considering the underlying simplifications in terms of adopted growth geometry. The accuracy of the proposed fit parameters is approximately ± 10 pct, *i.e.*, considering the experimental errors similar fit qualities can be obtained when the combinations of the three parameters are modified within this margin. As illustrated in a previous analysis,^[19] substantial changes in one of the parameters lead to significant deviations between the calculated and measured transformation kinetics that cannot be compensated by adjusting the two remaining parameters.

To evaluate the fundamental merits of the proposed model, it is important to critically analyze the values of the fit parameters given in Table II, as all three parameters have a well-defined physical meaning. The mobility factor is about a factor 2 smaller than that originally proposed by Krielaart and van der Zwaag^[28] for the Fe-Mn system, *i.e.*, 0.058 cm mol/J s, without, however, explicitly accounting for solute drag, *i.e.*, this original value reflects an effective rather than an intrinsic mobility. Considering previous work that accounted for solute drag mobility factors were concluded that are orders of magnitude larger and fall into the range of 450 to 3000 cm mol/J s.^[19,20,39] All these mobility values were obtained for Fe-alloys and ultra low-carbon steels with carbon contents of 0.007 wt pct or lower, whereas in the present case the carbon content is at least about an order of magnitude higher. These apparent mobility differences may thus be related to the different steel compositions, in particular the carbon content, as any solute atom in the iron lattice could affect the rate of the interface reaction from FCC to BCC crystal structure. Further studies will be required to quantify potential chemistry dependencies of the mobility factor.

The obtained activation energy Q_b locates the trans-interface diffusivity between the values for bulk diffusion of Nb in austenite and ferrite, respectively, as shown in Figure 8. The present result is consistent with the geometric average of D_γ and D_α for the trans-interface diffusivity as proposed by Zurob *et al.*^[13–15]

The binding energy of Nb is another important physical parameter that is used as an adjustable value

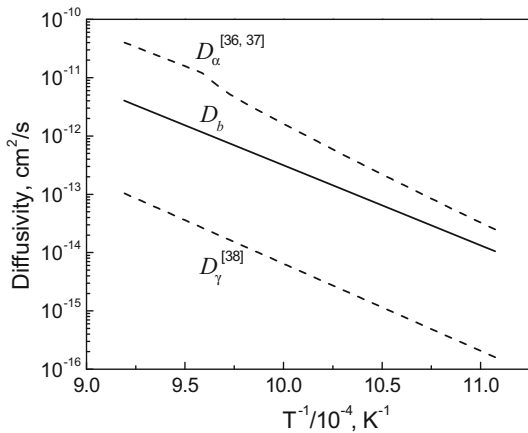


Fig. 8—Trans-interface diffusivity compared with bulk diffusion of Nb in austenite and ferrite.

in the present work. There are no direct experimental data available for the Nb binding energy to the austenite-ferrite interface but Nb segregation to ferrite grain boundaries has been studied experimentally and may be taken as a reference. Maruyama *et al.*^[40] used a 3-D atom probe study to measure the segregation of Nb to ferrite grain boundaries in an Fe-0.087 at. pct Nb alloy treated at 1073 K (800 °C). Their experimental result gives an interfacial Nb concentration of $9.7 \pm 2.7 \times 10^{17}$ atoms/m² with a segregation width of 1 to 2 nm. Using a wedge-shaped interaction potential across the grain boundary and an interface width of 2 nm, a Nb binding energy of 28.9 kJ/mol was calculated by Sinclair *et al.*^[41] In the present study, an interface width of 1 nm is assumed and then a binding energy of 36.7 kJ/mol is consistent with the experimental data of Maruyama *et al.*^[40] In addition, a recent density functional theory (DFT) calculation for the interaction of solutes with the $\Sigma 5$ ferrite grain boundary by Jin *et al.*^[42] gives binding energies for Nb to individual boundary sites in the range of 36 to 48 kJ/mol with an average of 39 kJ/mol which is a very similar value as that concluded from the atom probe study. The apparent binding energy of 48 kJ/mol obtained with the present model for Nb segregation at austenite-ferrite interfaces is of similar magnitude as the above values for grain boundary segregation.

IV. CONCLUSIONS

A combinatorial method which couples the mixed-mode reaction and solute drag of Nb has been used to model the austenite-to-ferrite transformation in a Nb microalloyed low-carbon steel. A description of the retarding effect of Nb on ferrite formation is obtained with an activation energy of 263 kJ/mol for Nb trans-interface diffusion and a Nb binding energy of 48 kJ/mol to the austenite-ferrite interface. The magnitude of these solute drag parameters is consistent with that expected from independent studies on diffusion and Nb grain boundary segregation reported in the literature. The trans-interface diffusivity used in the present model

supports the assumption to approximate its value by the geometric mean of bulk diffusion in austenite and ferrite as proposed by Zurob *et al.*^[13–15] Further, investigations are, however, required to confirm the generality of this assumption. A recent analysis of Qiu *et al.*^[15] indicates that different assumptions for the trans-interface diffusivity have to be made when considering the solute drag effect of Mn and Si, respectively, on the moving austenite-ferrite interface in Fe-C-Mn, Fe-C-Si and Fe-C-Si-Mn systems. Further, the so-called intrinsic interface mobility appears to be a function of steel chemistry and can presently only be employed as an adjustable parameter albeit an Arrhenius relationship for the mobility with an activation energy of 140 kJ/mol is in general applicable to low-alloyed Fe systems with sufficiently low carbon content.

The present model is applicable to the ferrite portion of the austenite decomposition. It will be critical to extend similar model approaches to describe the effect of Nb on the formation of bainitic ferrite as well. In the present case, the bainitic structures form above 773 K (500 °C) where a diffusional model for bainite growth may be appropriate such that a similar solute drag analysis could be considered. Modeling of bainite growth is, however, much more complex as growth anisotropies will have to be included.

ACKNOWLEDGMENTS

The authors thank the Natural Sciences and Engineering Research Council (NSERC) of Canada, the National Natural Science Foundation of China (Grant No. 51204048) and the Fundamental Research Funds for the Central Universities (Grant No. N120407008) for financial support. The steel was supplied by Essar Steel Algoma.

REFERENCES

1. A.J. DeArdo: *Int. Mater. Rev.*, 2003, vol. 48, pp. 371–402.
2. R.I. Rees, J. Perdrix, T. Maurickx, and H.K.D.H. Bhadeshia: *Mater. Sci. Eng. A*, 1995, vol. 194A, pp. 179–86.
3. X.Q. Yuan, Z.Y. Liu, S.H. Jiao, L.Q. Ma, and G.D. Wang: *ISIJ Int.*, 2006, vol. 46, pp. 579–85.
4. M.H. Thomas and G.M. Michal: in *Solid-Solid Phase Transformations*, H.I. Aaronson, D.E. Laughlin, R.F. Sekerka, and C.M. Wayman, eds., TMS-AIME, Warrendale, PA, 1981, pp. 469–73.
5. M. Suehiro, Z.K. Liu, and J. Ågren: *Acta Mater.*, 1996, vol. 44, pp. 4241–51.
6. C. Fossaert, G. Rees, T. Maurickx, and H.K.D.H. Bhadeshia: *Metall. Mater. Trans. A*, 1995, vol. 26A, pp. 21–30.
7. K.J. Lee and J.K. Lee: *Scripta Mater.*, 1999, vol. 40, pp. 831–36.
8. T. Furuhashi, T. Yamaguchi, G. Miyamoto, and T. Maki: *Mater. Sci. Technol.*, 2010, vol. 26, pp. 392–97.
9. G. Purdy, J. Ågren, A. Borgenstam, Y. Bréchet, M. Enomoto, T. Furuhashi, E. Gamsjäger, M. Gouné, M. Hillert, C. Hutchinson, M. Militzer, and H. Zurob: *Metall. Mater. Trans. A*, 2011, vol. 42A, pp. 3703–18.
10. A. Phillion, H.S. Zurob, C.R. Hutchinson, H. Guo, D.V. Malakhov, J. Nakano, and G.R. Purdy: *Metall. Mater. Trans. A*, 2004, vol. 35A, pp. 1237–42.
11. C.R. Hutchinson, A. Fuchsmann, H.S. Zurob, and Y. Bréchet: *Scripta Mater.*, 2004, vol. 50, pp. 285–90.

12. C.R. Hutchinson, H.S. Zurob, and Y. Bréchet: *Metall. Mater. Trans. A*, 2006, vol. 37A, pp. 1711–20.
13. H.S. Zurob, D. Panahi, C.R. Hutchinson, Y.J.M. Bréchet, and G.R. Purdy: *Metall. Mater. Trans. A*, 2013, vol. 44A, pp. 3456–71.
14. A. Béché, H.S. Zurob, and C.R. Hutchinson: *Metall. Mater. Trans. A*, 2007, vol. 38A, pp. 2950–55.
15. C. Qiu, H.S. Zurob, D. Panahi, Y.J.M. Bréchet, G.R. Purdy, and C.R. Hutchinson: *Metall. Mater. Trans. A*, 2013, vol. 44A, pp. 3472–83.
16. M. Militzer, M.G. Meozzi, J. Sietsma, and S. van der Zwaag: *Acta Mater.*, 2006, vol. 54, pp. 3961–72.
17. M.G. Meozzi, M. Militzer, J. Sietsma, and S. van der Zwaag: *Metall. Mater. Trans. A*, 2008, vol. 39A, pp. 1237–47.
18. F. Fazeli and M. Militzer: *Metall. Mater. Trans. A*, 2005, vol. 36A, pp. 1395–1405.
19. T. Jia and M. Militzer: *ISIJ Int.*, 2012, vol. 52, pp. 644–49.
20. E. Gamsjäger, M. Militzer, F. Fazeli, J. Svoboda, and F.D. Fischer: *Comput. Mater. Sci.*, 2006, vol. 37, pp. 94–100.
21. H. Chen, B. Appolaire, and S. van der Zwaag: *Acta Mater.*, 2011, vol. 59, pp. 6751–60.
22. M. Gómez, S.F. Medina, and G. Caruana: *ISIJ Int.*, 2003, vol. 43, pp. 1228–37.
23. J. Majta, A.K. Zurek, M. Cola, P. Hochanadel, and M. Pietrzyk: *Metall. Mater. Trans. A*, 2002, vol. 33A, pp. 1509–20.
24. E. Gamsjäger, J. Svoboda, and F.D. Fischer: *Comput. Mater. Sci.*, 2005, vol. 32, pp. 360–69.
25. E. Gamsjäger, H. Chen, and S. van der Zwaag: *Comput. Mater. Sci.*, 2014, vol. 83, pp. 92–100.
26. M.G. Meozzi, J. Sietsma, and S. van der Zwaag: *Acta Mater.*, 2006, vol. 54, pp. 1431–40.
27. Y. Takahama and J. Sietsma: *ISIJ Int.*, 2008, vol. 48, pp. 512–17.
28. G.P. Krielaart and S. van der Zwaag: *Mater. Sci. Technol.*, 1998, vol. 14, pp. 10–18.
29. H. Strandlund, J. Odqvist, and J. Ågren: *Comput. Mater. Sci.*, 2008, vol. 44, pp. 265–73.
30. S. Gerami: Master's Thesis, University of British Columbia, Vancouver, 2010.
31. H.K.D.H. Bhadeshia, S.A. David, J.M. Vitek, and R.W. Reed: *Mater. Sci. Technol.*, 1991, vol. 7, pp. 686–98.
32. J.S. Park, Y.S. Ha, S.J. Lee, and Y.K. Lee: *Metall. Mater. Trans. A*, 2009, vol. 40A, pp. 560–68.
33. M. Militzer, R. Pandi, and E.B. Hawbolt: *Metall. Mater. Trans. A*, 1996, vol. 27A, pp. 1547–56.
34. M. Militzer, F. Fazeli, and H. Azizi-Alizamini: *Metall. Ital.*, 2011, vol. 103, pp. 35–41.
35. M. Militzer, F. Fazeli, and T. Jia: *Fundamentals and Applications of Mo and Nb Alloying in High Performance Steels: Volume 1*, H. Mohrbacher, ed., CBMM/IMOA/TMS, 2014, pp. 23–36.
36. J. Geise and C. Herzig: *Z. Metall.*, 1985, vol. 76, pp. 622–26.
37. C. Herzig, J. Geise, and S.V. Divinski: *Z. Metall.*, 2002, vol. 93, pp. 1180–87.
38. S. Akamatsu, T. Senuma, and M. Hasebe: *ISIJ Int.*, 1992, vol. 32, pp. 275–82.
39. E. Kozeschnik and E. Gamsjäger: *Metall. Mater. Trans. A*, 2006, vol. 37A, pp. 1791–97.
40. N. Maruyama, G.D.W. Smith, and A. Cerezo: *Mater. Sci. Eng. A*, 2003, vol. 353A, pp. 126–32.
41. C.W. Sinclair, C.R. Hutchinson, and Y. Bréchet: *Metall. Mater. Trans. A*, 2007, vol. 38A, pp. 821–30.
42. H. Jin, I. Elfmov, and M. Militzer: *J. Appl. Phys.*, 2014, vol. 115, pp. 093506 (8 pp).